

Pore characterization, acoustic and permeability measurements on core plug triplets, from the Miocene Tótkomlós (Calcareous Marl) Formation of the Pannonian-basin, Hungary

Péter Koroncz¹, Péter Ács¹, Viktor Lemberkovics² and Ferenc Fedor¹

¹ GEOCHEM Ltd., Viola str. 55/1., H-7761 Kozármisleny, Hungary; (geochem@geochem-ltd.eu)

² RAG Hungary Ltd., Bocskai rd. 134-146., H-1113 Budapest, Hungary; (Viktor.Lemberkovics@rag-hungary.hu)

doi: 10.4154/gc.2017.09



Article history:

Manuscript received January 31, 2017

Revised manuscript accepted May 26, 2017

Available online June 28, 2017

Abstract

The Tótkomlós Calcareous Marl (TCM), a Member of the Late Miocene Endrőd Formation was investigated as a potential cap and source rock and also as a local tight reservoir in the Pannonian Basin. Only a limited dataset is available for petrophysical characterisation of this formation. The study reports on a complex measurement campaign performed on three core triplet samples of the Tótkomlós Calcareous Marl, including pore structure and petrophysical analysis at various pressure conditions. Direct laboratory measurements of compressional (P) and shear (S) wave velocities on oriented rock samples provide information about the anisotropic behaviour of the studied samples. A quantitative description of seismic anisotropy can improve the quality of seismic data processing.

Pore structure investigations indicated plate-like materials with a typical pore throat size between 75–110 nm. Gas permeability measurements showed very low permeability values in the order of magnitude between 10^{-16} – 10^{-18} m². Weak acoustic anisotropy is observed both for P- and S-waves. Decreasing anisotropy with increasing confining pressure indicated that the samples become less anisotropic with increasing effective stress.

Keywords: calcareous marl, acoustic anisotropy, pore structure

1. INTRODUCTION AND GEOLOGICAL SETTING

The investigated well is located in the southern part of the Danube-Tisza Interflow, Hungary. Samples for analysis were taken from the lower Pannonian age basal marl succession, namely from the Endrőd Marl Formation (JUHÁSZ, 1992; 1998). This basal marl sequence is an initial member of the Pannonian-Pliocene age prograding – dominantly siliciclastic – lacustrine self-system (MAGYAR et al., 2013). In the early stage of deposition due to the rapid thermal subsidence of the Pannonian basin, a so called „starved” sedimentation phase formed in the basin. During this stage, the siliciclastic sediment input was limited to the edges of the depocentre and a carbonate rich sequence was deposited almost throughout the Pannonian basin area. This sequence generally began with a high carbonate content calcareous marl, to marl sequence (Tótkomlós Calcareous Marl Member) overlain by a deep water, pelagic clay-marl sequence (Nagykörű Claymarl Member), developed with a continuous transition from the underlying carbonate rich rocks (JUHÁSZ, 1992; 1998). The carbonate content decreases upwards, caused by the increasing terrigenous material input (due to the prograding shelf-system), providing a characteristic and easy to recognize wireline pattern (Figure 1).

In the study area, the calcareous marl-marl sequence developed almost everywhere except for the south-western, shallowest part of the basin (Figure 2).

The calcareous marl has several lithofacies, but in general dark grey, black, laminated-microlaminated facies were deposited in the deep basin areas, while under the shallow water conditions light grey – yellowish or brownish grey, whitish coloured, massive or laminated facies accumulated (JUHÁSZ, 1992; 1998; LEMBERKOVICS, 2016). The investigated samples represent

the shallow water facies (Figure 2. represents approximately the palaeo-geomorphology on which deposition of the calcareous marl occurred). Their colour is generally yellowish grey to grey, mainly massive, but sometimes laminated, occasionally organic rich bands, layers of few – ten centimetres scale carbonate rich sandstone layers are interbedded with the monotonous calcareous marl in the core samples (Figure 3).

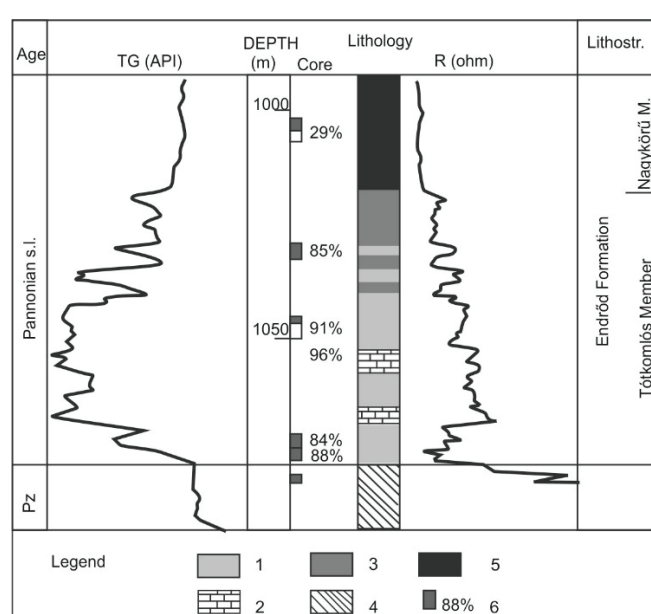


Figure 1. A typical log pattern of the Tótkomlós Calcareous Marl Member as recorded in a Battonya borehole. 1. calcareous marl, 2. limestone, 3. marl, 4. metamorphic basement, 5. clay-marl, 6. core sample with the measured carbonate content (modified after MAGYAR et al., 2001).

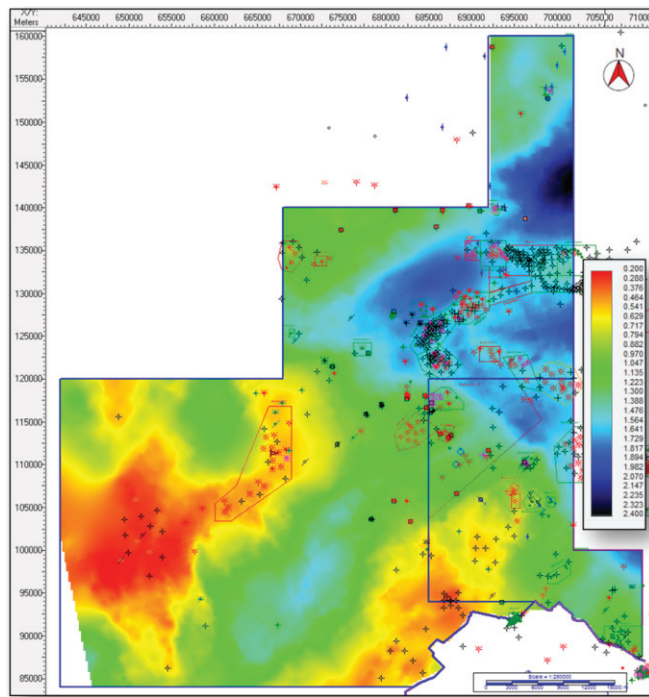


Figure 2. Basal Pannonian (Base Calcareous Marl Member) TWT seismic depth map of the study area. The investigated well is highlighted with the red circle. Calcareous marl is non-deposited or eroded at the reddish coloured acreages (LEMBERKOVICS, 2016).

2. THEORETICAL BACKGROUND OF THOMSEN'S ANISOTROPY PARAMETERS

In the case of elastic materials, the relationship between stress and strain can be described by Hooke's law (AULD, 1973):

$$\sigma_{ij} = C_{ijkl} \varepsilon_{kl} \quad (1)$$

where:

σ – the second-rank stress tensor

ε – the second-rank strain tensor

i, j and k, l = 1, 2, 3 indicating one of three orthogonal axes

C – the fourth-rank stiffness tensor with 81 tensor components

Symmetry of the stress and strain tensors, as well as internal energy arguments lead to reduction of the number of independent elements to 21 (HEMSING, 2007).

Elastic properties of shales and shale-type rocks (as well as calcareous marls) are known to be anisotropic, typically considered to have a Transversely Isotropic (or hexagonal) symmetry with a symmetry axis perpendicular to the bedding plane. The

main sources of anisotropy are layering (TI symmetry), the preferred orientation of clay minerals, microcracks and pores.

In the case of vertically transversely isotropic (VTI) materials with hexagonal symmetry, the stiffness tensor could be described by 5 independent tensor components.

$$C_{IJ} = \begin{bmatrix} C_{11} & C_{11}-2C_{66} & C_{13} & 0 & 0 & 0 \\ C_{11}-2C_{66} & C_{11} & C_{13} & 0 & 0 & 0 \\ C_{13} & C_{13} & C_{33} & 0 & 0 & 0 \\ 0 & 0 & 0 & C_{44} & 0 & 0 \\ 0 & 0 & 0 & 0 & C_{44} & 0 \\ 0 & 0 & 0 & 0 & 0 & C_{66} \end{bmatrix} \quad (2)$$

Elastic constants (C_{11} , C_{33} , C_{44} , C_{66} , C_{13}) that describe a VTI medium as a function of phase velocities are given by THOMSEN (1986):

$$C_{11} = \rho V_{P,90}^2 \quad (3)$$

$$C_{33} = \rho V_{P,0}^2 \quad (4)$$

$$C_{44} = \rho V_{S,0}^2 \quad (5)$$

$$C_{66} = \rho V_{SH,90}^2 \quad (6)$$

$$C_{13} = -C_{44} + \left[\frac{(4\rho V_{P,45}^2 - C_{11} - C_{33} - 2C_{44})^2 - (C_{11} - C_{33})^2}{4} \right]^{1/2} \quad (7)$$

where $V_{P,90}$, $V_{P,0}$, $V_{S,0}$ and $V_{SH,90}$ are the compressional and shear wave velocities measured in the different orientations according to Figure 5. and ρ is the bulk density of the sample.

Thomsen's anisotropy parameters (ε , γ , δ) which are usually used in depth migration in seismics are dimensionless combinations of elastic moduli that characterize transversely isotropic materials. They are defined in the following way:

$$\varepsilon = \frac{C_{11} - C_{33}}{2C_{33}} \quad (8)$$

$$\gamma = \frac{C_{66} - C_{44}}{2C_{44}} \quad (9)$$

$$\delta = \frac{(C_{13} + C_{44})^2 - (C_{33} - C_{44})^2}{2C_{33}(C_{33} - C_{44})} \quad (10)$$

where ε is the P-wave anisotropy factor, γ is the SH-wave anisotropy factor and δ is a more complicated expression that may be interpreted as a measure of the anellipticity of the P wave curve (CHOLACH & SCHMITT, 2006). As THOMSEN (1986) de-

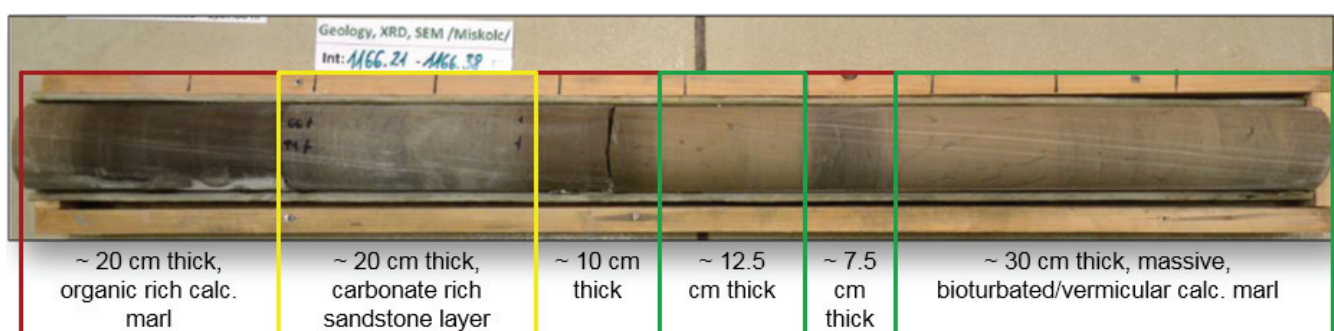


Figure 3. Core photo and its macroscopic description of the investigated sediments. Various rock types or subfacies were identified in the calcareous marl sequence (LEMBERKOVICS, 2016). The colour code of the rectangles highlights the same rock facies.

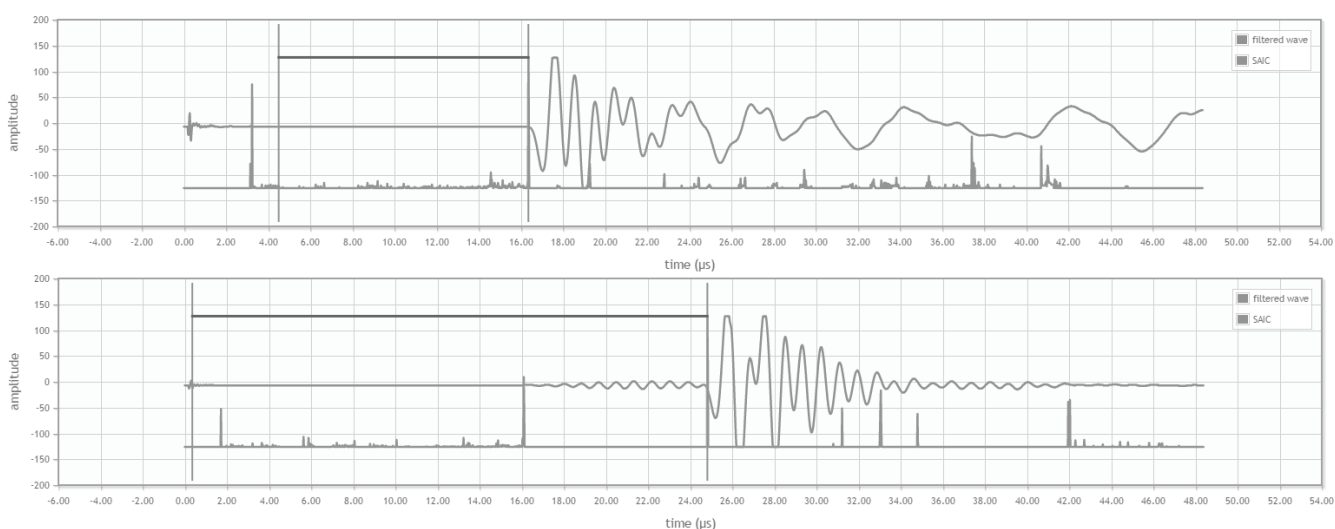


Figure 4. A typical record of compressional (above) and shear (below) waveforms with first-break detection using a modified Akaike Information Criteria (SAIC) algorithm.

scribed, δ is the difference between the smallest offset normal moveout (NMO) velocity and vertical velocity to interpret the small AVO response (TSVANKIN, 1997; OSTADHASSAN et al., 2012).

Depth migration algorithms in seismic processing require Thomsen's ϵ and δ values, and these parameters can reliably be calculated from direct laboratory measurements. In the case of sedimentary rocks, values of ϵ , γ and δ are generally in the same order of magnitude, usually smaller than 0.2. Moreover, the values are typically higher than 0 in most rocks but negative values are also possible (THOMSEN, 1986).

3. SAMPLES

Three plug-triplet samples were taken from a homogenous part of the calcareous marl core sections and are macroscopically characterised in Table 1.

Table 1. Macroscopic description of investigated core sections.

S-01	Light brown calcareous marl bands (thickness 1-3 cm). Transitions from the lighter bands to the darker ones are continuous.
S-02	Light yellowish-greyish brown calcareous marl with disperse organic matter.
S-03	Greyish brown, homogenous calcareous marl .

4. TEST METHODS

An ultrasonic pulse-transmission technique was used to determine the P- and S-wave velocities. In this case two transducers are placed on the end faces of the samples. The frequency of the transducers used for measurements was centred around 1 MHz, both for compressional and shear waves. Travel times for velocity data were determined with a „first-break” record (Figure 4). For an accurate and exact determination of flying times, a new algorithm was developed based on the Akaike Information Criteria (AKAIKE, 1973; KORONCZ & FEDOR, 2016). Previous studies (e.g. DELLINGER & VERNIK, 1994; HORNBY, 1998) confirmed that ultrasonic laboratory measurements represent phase velocities.

For the analysis of acoustic anisotropy, a multicore test method was used. In this case, multiple 1" diameter plugs were drilled parallel (90°), perpendicular (0°) and at 45° to bedding planes from a larger sample (Figure 5).

Multi-core methods have been used by many authors to quantify anisotropy (e.g. JOHNSTON & CHRISTENSEN, 1995; VERNIK & LIU, 1997; HEMSING, 2007) however there are disadvantages of the multi-core method. For example, coring may sample different heterogeneities of the material (HEMSING, 2007).

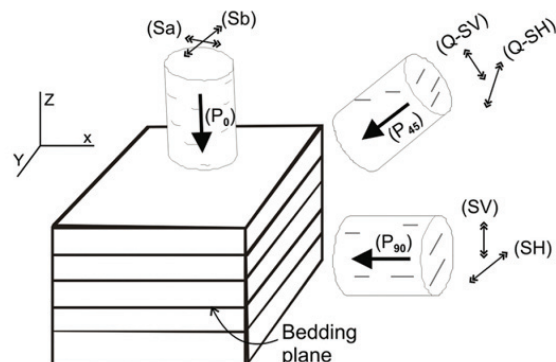


Figure 5. Schematic figure of multicore sampling with the polarization directions of shear wave transducers used for velocity measurements (MARTÍNEZ & SCHMITT, 2011).

For the investigation of the effect of effective stress, measurements were carried out in a high pressure triaxial cell in the range of 0-50 MPa effective stress using 5 MPa pressure increments.

Plugs were dried at 60°C to preserve the chemically bound water in the lattice of clay minerals, and were stored in a desiccator before measurement. In order to prevent contamination of samples, coupling media were not used. Due to the low coupling, measurement error is slightly higher at 0 Mpa effective stress. At higher confining pressures, the RMS (root-mean-square) error of velocities was less than 1%.

For investigating the stress sensitive behaviour of porosity, „Boyle’s law Single Cell Method“ (API, 1998) was used to determine porosity using 10 MPa pressure steps. Helium gas permeabilities were also measured with the „Pressure-Falloff, Axial Gas Flow measurement technique“ (API, 1998) at a constant pressure of 15 MPa.

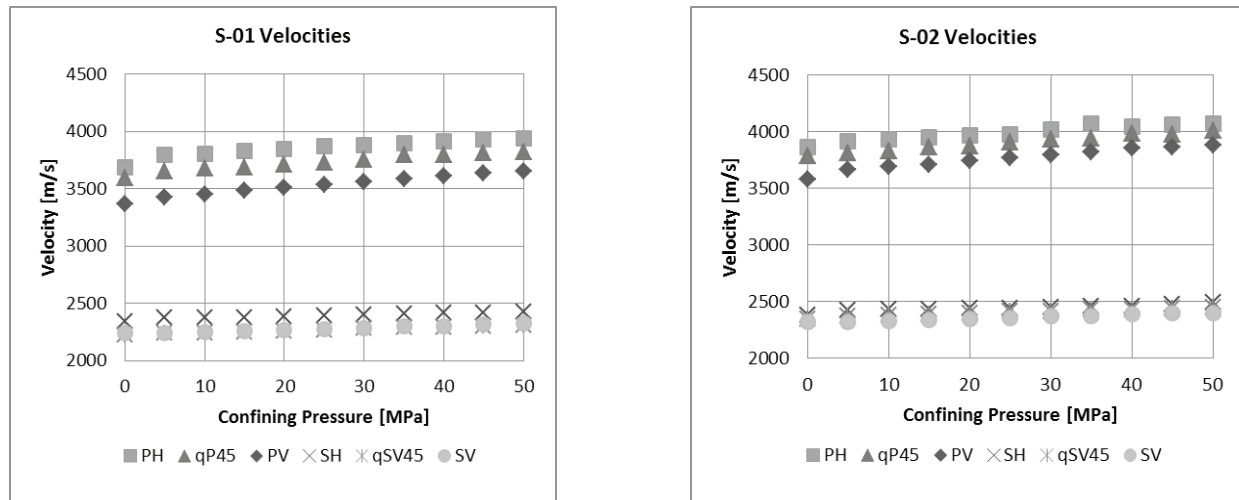


Figure 6. Acoustic wave velocities of cores with different orientations at Sample-01 and -02.

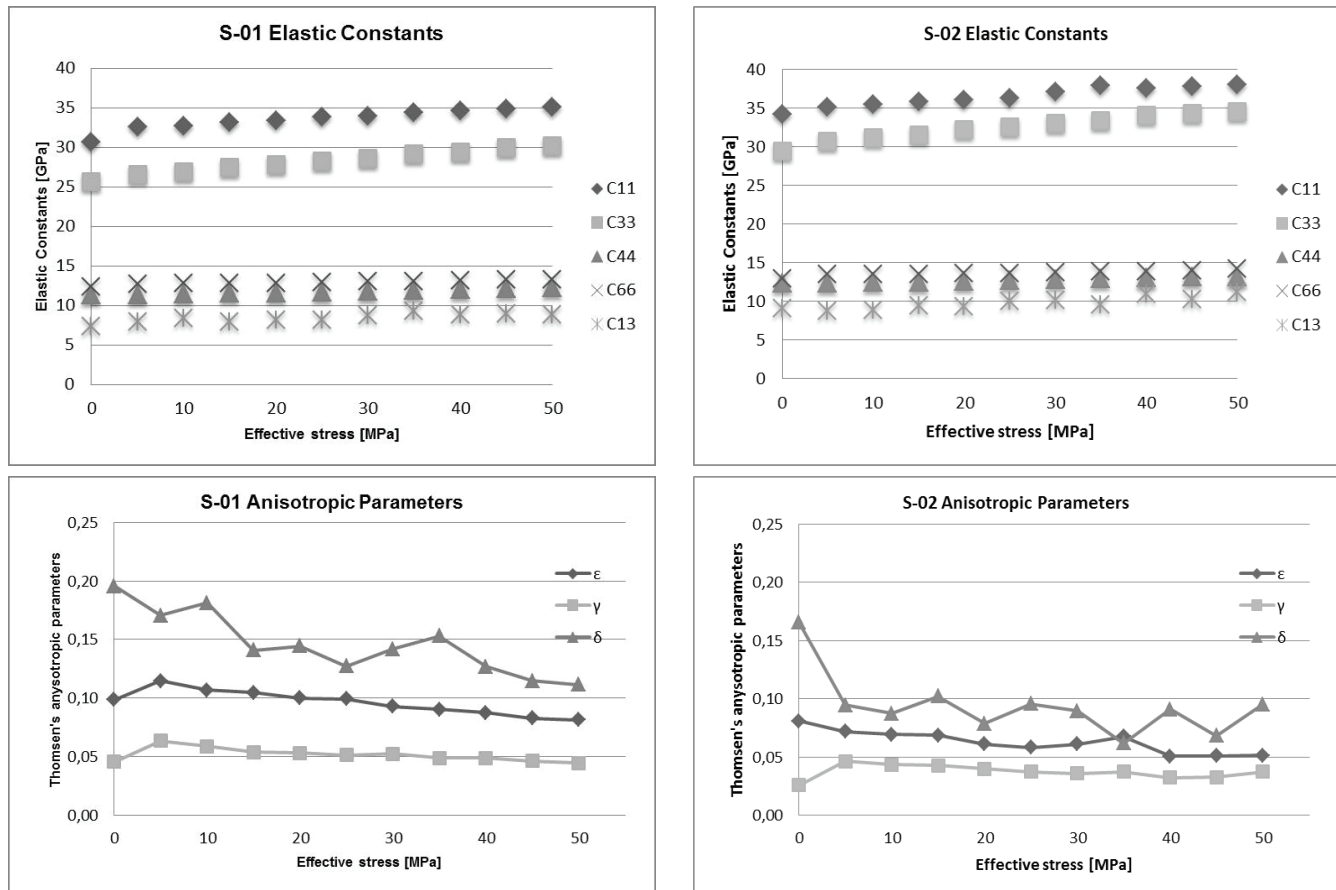


Figure 7. Calculated elastic constants and anisotropic parameters as a function of effective stress.

For pore structure measurements, plugs with different diameters (1", 9 mm) were studied. Every sample was dried at 60 °C in a drying oven for a week prior to measurement.

The skeletal volume of plugs with 1" diameters were measured at 25 °C with a Pentapyc 5200e (PPY-30T) instrument. Knowing the geometric volume and the skeletal volume, the helium porosity (ϕ_{He}) of the plugs was calculated. Skeletal density (ρ_{skeletal}) and bulk density (ρ_{bulk}) were also calculated from the measured data.

The N₂ and CO₂ adsorption-desorption isotherms of small plugs (9 mm diameter) were measured with a Quantachrome Au-

tosorb AS-1 instrument. After the drying process the samples were outgassed for 24 h at 60 °C before measurement. Physisorption tests were carried out with N₂ (at 77 K) and CO₂ (at 273 K) gases, in the case of N₂ gas BET (Brunauer-Emmett-Teller method) surface area (S_{BET}), total pore volume (V_{tot}) parameters were calculated. The CO₂ gas is very useful for exploring the micropore structure of the samples (CAZORLA-AMOROS et al., 1996), the micropore surface area (S_{mic}) and micropore volume (V_{mic}) were determined with the Dubinin-Radushkevich method.

A Quantachrome Poremaster-60 GT instrument was used during the mercury intrusion porosimetry (MIP) tests. The maxi-

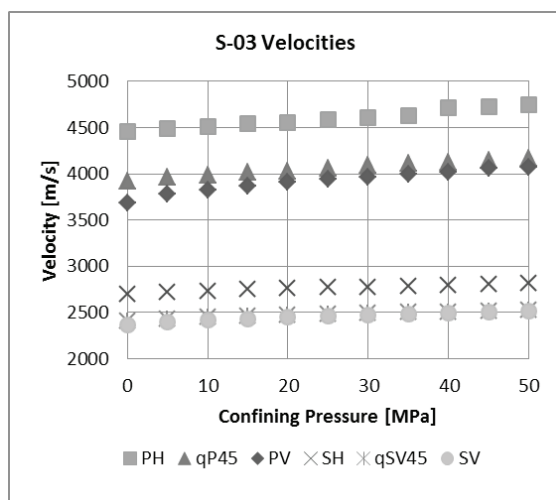


Figure 8. Acoustic velocity measurements of Sample-03.

mum (420 MPa) and minimum (1.5 kPa) applied pressure corresponds to cylindrical pore sizes of 3 nm and 800 μm , respectively. Contact angles were determined with a mercury contact angrometer (Quantachrome) as an average value of three independent measurements. MIP was used to investigate the pore throat size distribution in the macro- and mesopore region as well as the mercury porosity (ϕ_{Hg}) and surface area (S_{Hg}) of the samples.

5. RESULTS AND INTERPRETATION

Figure 6. shows acoustic velocity measurements as a function of confining pressure. All of the cores show an increase in velocity

with increasing pressure. This is the result of self-sealing, as pores and microcracks begin to close when a sample is pressurized. Plugs drilled parallel to bedding show higher velocities than cores drilled perpendicularly to bedding. The velocities of 45° cores were between these values.

Velocities perpendicular to bedding increase more with pressure, which could suggest that pores in the samples are aligned horizontally (MARTÍNEZ et al., 2012).

Figure 7. presents the calculated elastic constants and anisotropy parameters as a function of effective stress in the case of Sample-01 and Sample-02.

Weak anisotropy is observed in both samples, Sample-01 showing slightly higher anisotropy values compared to Sample-02. For Sample-01 compressional wave anisotropy (ε) measured at 5 MPa is up to 11.5%, while shear wave anisotropy (γ) of 6.5% was observed. Both P- and S-wave anisotropy (ε, γ) decreased with increasing confining pressure, so indicating that the samples become less anisotropic with increasing effective stress.

In the case of the third plug-triplet (Sample-03) higher anisotropy could be observed (Figure 8). Although macroscopically no difference could be observed between the samples, the much lower porosity (5.07 %) in the case of sample S-03-90° (drilled parallel to bedding planes) indicated that plug-triplets may not represent the same rock type. The explanation of this phenomenon requires a more detailed petrological characterization (including thin section analysis, XRD, DTA) in the future.

Gas permeability measurements indicate very low permeability values in the order of magnitude between 10^{-16} - 10^{-18} m^2 . Since pressure fall-off permeability data are less reliable in such

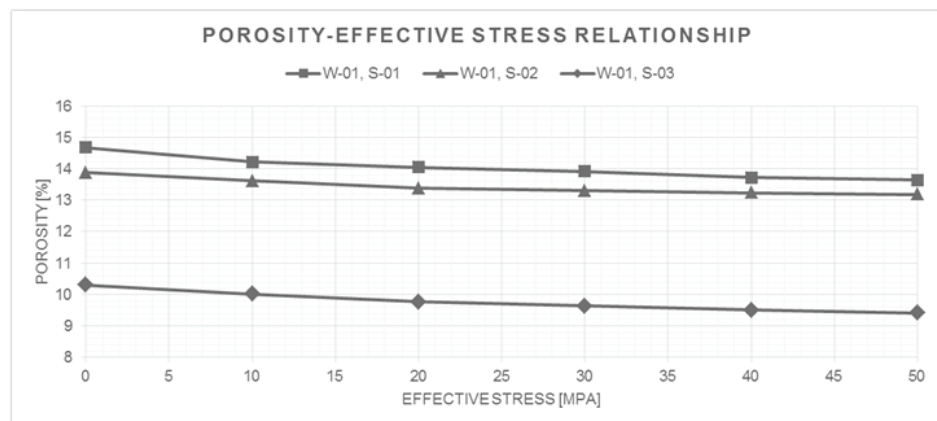


Figure 9. Porosity reduction due to increasing effective stress in the case of samples perpendicular to bedding.

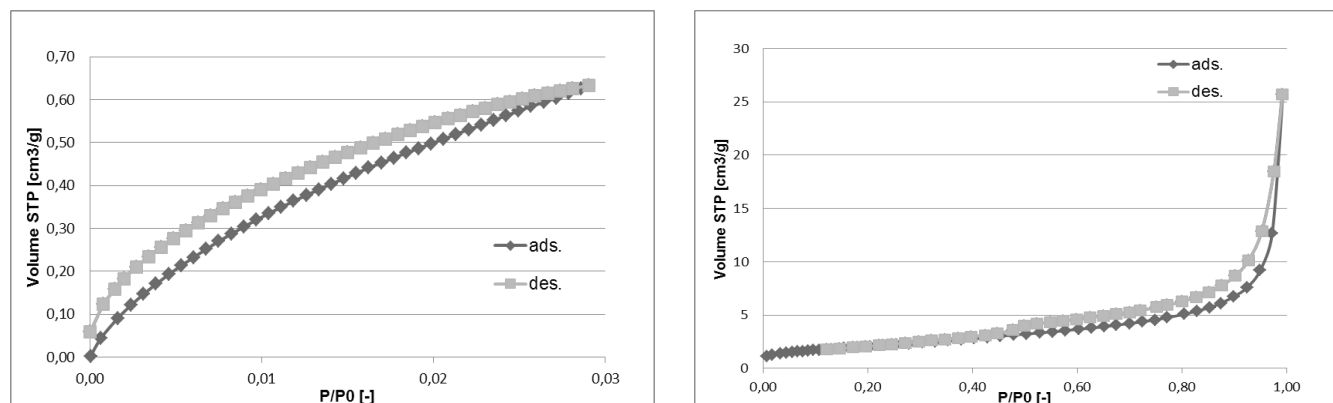


Figure 10. Typical CO₂ (left) and N₂ (right) adsorption-desorption isotherms of plugs.

a low permeability range, these measurements will be measured in a future work by a pressure pulse decay (PPD) technique that provides more accurate results in the case of permeabilities lower than 10^{-15} m^2 (FEDOR et al., 2008).

The decrease of porosity is clearly observed during measurements as Figure 9. shows. Initial porosity values of tested samples vary between 10-15 % (Table 2). Porosity reduction due to increasing effective stress can reach 10% in the 50 MPa range.

Table 2. Test results of He-pycnometry measurements.

sample ID	ρ_{skeletal} [g/cm ³]	ρ_{bulk} [g/cm ³]	Φ_{He} [%]
S-01	2.6591±0.0072	2.259±0.013	15.06±0.71
S-02	2.6524±0.0043	2.296±0.012	13.43±0.45
S-03*	2.6573*	2.433*	10.16*

*remark: only two samples were measured

The adsorption isotherms of the samples can be classified in the Type II IUPAC (International Union of Pure and Applied Chemistry) class, which is related to macroporous materials (Figure 10). Hysteresis was observed on all isotherms. The shape of the hysteresis loop is similar with H3 type according to the IUPAC classification. The H3 loop is often associated with Type II isotherms and is related to non-rigid aggregates of plate-like materials (THOMMES, 2015). In addition, macropores that are not completely filled with pore condensate also caused such a hysteresis loop. The main pore throat size is between 75-110 nm according to the mercury porosimetry measurements.

Calculated Hg-porosity (ϕ_{Hg}) values are lower than the He-porosity values (ϕ_{He}) indicating micropores (<2 nm pore diameter) in the pore structure. Besides, the S_{BET} values are also higher than S_{Hg} which also suggests the presence of micropores (Table 3).

Table 3. Test results of pore structure investigations.

sample ID	Physisorption			Hg-porosimetry		
	N ₂		CO ₂	S_{BET} [m ² /g]	V_{tot} [cm ³ /g]	V_{mic} [cm ³ /g]
S-01	7.74	4.26E-02	2.82E-03	8.10	4.66	9.33E-02
S-02	5.60	3.38E-02	2.04E-03	5.84	4.24	7.79E-02
S-03	7.61	3.99E-02	2.93E-03	8.40	4.76	1.09E-01

6. CONCLUSIONS

A detailed petrophysical investigation was performed on 3 plug-triplets drilled from the Tótkomlós Calcareous Marl section, including acoustic anisotropy and complex pore structure characterization.

Using the multicore test method, acoustic wave velocities were measured at different confining pressures. Based on accurate velocity measurements on plugs with different orientations, anisotropy could be described in a quantitative way. These parameters could be applied in seismic depth migration. Porosity measurements showed porosity reduction as a function of increasing effective stress. Pore structure investigations indicated plate-like materials with a typical pore throat size between 75-110 nm. Micropores (<2 nm pore diameter) were also observed in the pore space.

In conclusion, self-sealing in marl could be observed during the measurements. PPD permeability measurements under rese-

rvoir conditions parallel with ultrasonic velocity measurements would help to track and understand the process and hence petrophysically characterize marls of sedimentary basins.

REFERENCES

- AKAIKE, H. (1973): Information theory and an extension of the maximum likelihood principle.– In: PETROV, B.N. & CSAKI, F. (eds.): Second international symposium on information theory. Akadémiai Kiadó, Budapest, 267–281.
- AMERICAN PETROLEUM INSTITUTE (1998): Recommended Practices for Core Analysis – API Publishing Services, Washington.
- AULD, B.A. (1973): Acoustic fields and waves in solids.– John Wiley & Sons Inc, New York, 423 p.
- CAZORLA-AMOROS, D., ALCANIZ-MONJE, J. & LINARES-SOLANO, A. (1996): Characterization of Activated Carbon Fibers by CO₂ Adsorption.– Langmuir, 12, 2820–2824. doi: 10.1021/la960022s
- CHOLACH, P.Y. & SCHMITT, D.R. (2006): Intrinsic elasticity of a textured transversely isotropic muscovite aggregate: Comparisons to the seismic anisotropy of schists and shales.– Journal of Geophysical Research, 111, 410–427. doi: 10.1029/2005JB004158
- DELLINGER, J. & VERNIK, L. (1994): Do traveltimes in pulse-transmission experiments yield anisotropic group or phase velocities?– Geophysics, 59, 1774–1779. doi: 10.1190/1.1443564
- FEDOR, F., HÁMOS, G., JOBBIK, A., MÁTHÉ, Z., SOMODI, G. & SZÜCS, I. (2008): Laboratory pressure pulse decay permea Laboratory Pressure Pulse Decay Permeability Measurement of Buda Claystone, Mecsek Mts, SW Hungary.– Physics and Chemistry of the Earth, 33, S45–S53.
- HEMSING, D.B. (2007): Laboratory determination of seismic anisotropy in sedimentary rock from the Western Canadian Sedimentary Basin: M.Sc. thesis, University of Alberta.
- HORNBY, B.E. (1998): Experimental laboratory determination of the dynamic elastic properties of wet, drained shales.– Journal of Geophysical Research, 103, 29945–29964. doi: 10.1029/97JB02380
- JOHNSTON, J.E. & CHRISTENSEN, N.I. (1995): Seismic anisotropy of shales.– Journal of Geophysical Research, 100, 5991–6003. doi: 10.1029/95JB00031
- JUHÁSZ, GY. (1992): A pannóniai (s.l.) formációk térképezése az Alföldön: elterjedés, facies és tizedékes környezet [Pannonian (s.l.) lithostratigraphic units in the Great Hungarian Plain: distribution, facies and sedimentary environment – in Hungarian].– Földtani Közlöny, 122/2–4, 133–165.
- JUHÁSZ, GY. (1998): A magyarországi neogén mélymedencék pannóniai képződményeinek litosztratigráfiaja [Lithostratigraphy of Pannonian Formations of Hungarian Neogene basins – in Hungarian].– In: JAMBOR et al.: Magyarország geológiai képződményeinek rétegtana, Budapest, 469–483.
- KORONCZ, P. & FEDOR, F. (2016): Experimental investigation of stress-dependent petrophysical behaviour of reservoir rocks.– In: CVETKOVIĆ et al. (eds.): 8th Croatian-Hungarian and 19th Hungarian geomathematical congress, Trakošćan, 83–87.
- LEMBERKOVICS, V. (2016): Distribution and heterogeneity of Tótkomlós Calcareous Marl Member of Endrőd Marl Formation, Kiskunhalas & Kelebia Exploration areas – Mészmađra Ankét Szolnok – verbal presentation, 11 slides.
- MAGYAR, I., JUHÁSZ, GY., SZUROMINÉ KORECZ, A. & SÜTÖNÉ SZENTAI, M. (2004): A pannóniai Tótkomlói Mészmađra Tagozat kifejlődése és kora a Battonya-pusztaföldvári-hátság környezetében [The Tótkomlós Calcareous Marl Member of the Lake Pannon sedimentary sequence in the Battonya-Pusztaföldvár region, SE Hungary – in Hungarian].– Földtani Közlöny, 133/4, 521–540.
- MAGYAR, I., RADIVOJEVIĆ, D., SZTANÓ, O., SYNAK, R., UJSZÁSZI, L. & PÓCSIK, M. (2013): Progradation of the paleo-Danube shelf margin across the Pannonian Basin during the Late Miocene and Early Pliocene.– Global and Planetary Change, 103, 168–173. doi: 10.1016/j.gloplacha.2012.06.007
- MARTÍNEZ, J.M. & SCHMITT, D. (2011): Investigating anisotropy in rocks by using pulse transmission method.– Canadian Society of Exploration Geophysicists Recorder, 36/10, 38–43.
- MARTÍNEZ, J.M., SCHMITT, D.R. & KOFMAN, R. (2012): Anisotropy measurements in a multi-faced core sample by using pulse transmission method, GeoConvention, Calgary, Alberta.
- OSTADHASSAN, M., ZENG, Z., JABBARİ, H. (2012): Anisotropy Analysis in Shale Using Advanced Sonic Data – Extended abstract, Bakken Case Study, AAPG Annual Convention and Exhibition, USA.
- THOMMES, M., KANEKO, K., NEIMARK, A.V., OLIVIER, J.P., RODRIGUEZ-REINOSO, F., ROUQUEROL, J. & SING, K.S.W. (2015): Physisorption of gases, with special reference to the evaluation of surface area and pore size distribution (IUPAC Technical Report).– Pure and Applied Chemistry, 87, 9–10, 1051–1069. doi: 10.1515/pac-2014-1117
- THOMSEN, L. (1986): Weak elastic anisotropy.– Geophysics, 51, 1954–1966. doi: 10.1190/1.1442051
- TSVANKIN, I. (1997): Reflection move-out and parameter estimation for horizontal transverse isotropy.– Geophysics, 62, 614–629. doi: 10.1190/1.1444170
- VERNIK, L. & LIU, X. (1997): Velocity anisotropy in shales: A petrophysical study.– Geophysics, 62, 521–532. doi: 10.1190/1.1444162